Supporting Information

Electron Tomography Reveals the Active Phase-Support Interaction in Sulfidic Hydroprocessing Catalysts

Sonja Eijsbouts†*, Xuanqi Li‡, Jana Juan-Alcaniz†, Leon C. A. van den Oetelaar†, Jaap A. Bergwerff†, Joachim Loos‡, Anna Carlsson§ and Eelco T. C. Vogt†

† Albemarle Catalysts Company B.V., Research Centre Amsterdam, P.O. Box 37650, Nieuwendammerkade 1-3, 1030 BE Amsterdam, The Netherlands,

‡ DSM Resolve, Chemelot Campus, Urmonderbaan 22, 6167 RD Geleen, The Netherlands,

§ Thermo Fischer Scientific, Achtseweg Noord 5, 5651 GG Eindhoven, The Netherlands.

Corresponding Author: * Dr. S. Eijsbouts, Albemarle Catalysts Company B.V., P.O. Box 37650, 1030 BE Amsterdam, The Netherlands, Email: Sonja.Eijsbouts@Albemarle.com.

Table of Contents

1 Experimental section

1.1.1 Fresh catalyst preparation

The TiO_2-Al_2O_3 mixed oxide support was prepared by standard coprecipitation of titanyl sulfate, aluminum sulfate and sodium aluminate. An explorative Ni-Mo/Al_2O_3-TiO_2 catalyst was prepared by coimpregnation of Ni and Mo on coprecipitated Al_2O_3-TiO_2 support (containing ca. 20 wt.% TiO_2 and 80 wt.% Al_2O_3) followed by drying at 120°C. The final catalyst contains 4.1 wt% NiO, 20.6 wt% MoO_3 and 13.9 wt% TiO_2 (balance is Al_2O_3). Ni/Mo atomic ratio of the active phase is 0.38. The fresh oxidic catalyst has a BET surface area of 244 m^2/g and pore volume of 0.46 cm^3/g. Pore size distribution is slightly bimodal, containing some micropores. Based on the BET surface area, it can be calculated that the Ni and Mo surface loadings are 1.4 and 3.6 atoms/nm^2, respectively.

1.1.2 Catalyst testing

The catalyst was sulfided in the liquid phase and tested in a Ultra Low Sulfur Diesel (ULSD) test (290-340°C, LHSV = 2-3 h^{-1}, H_2:oil = 300 Nl/l, 45 bar, time on stream = 12 days). The Ni-Mo/Al_2O_3-TiO_2 showed a satisfactory performance [relative volume activity (RVA) in hydrodesulfurization (HDS) of about 60% and hydrodenitrogenation (HDN) of about 70% as compared to the commercial Ni-Mo/Al_2O_3 reference].

1.1.3 Used catalyst

The used Ni-Mo/Al_2O_3-TiO_2 catalyst from the ULSD test was unloaded in a flask filled with diesel oil and stored under diesel oil to prevent reoxidation of this sulfidic material by air prior to any further analysis.

1.1.4 Characterization Techniques

The catalysts were characterized by (Scanning) Transmission Microscopy with Energy dispersive X-ray spectroscopy (STEM-EDX). In addition to that, 3D High-Angle Annular Dark Field (HAADF) STEM-HAADF measurements have been carried out.

1.1.5 STEM-EDX and 3D-STEM-HAADF

Specimen preparation for 2D TEM and STEM-EDX measurements: The sample was briefly rinsed with toluene, ground in a mortar and dried at 150 °C (to remove residual toluene) in Pfeiffer vacuum impregnation equipment. After drying, the samples was embedded in Ultra Low Viscosity Kit (ULVK) epoxy resin and cured at 60 °C under pressure (2.5 bar) for at least 48 hours. After curing, sections with a thickness of about 60 nm have been obtained by microtome cutting at room temperature. Sections were collected on a water surface, and transferred to carbon coated grids (400 mesh grids).

Specimen preparation for 3D STEM-HAADF measurements: The sample was rinsed with toluene and finely ground in a mortar. After drying, the ground sample was dispersed in ethanol. One droplet of the suspension was dropped on the carbon coated 200 mesh grid and dried in fume hood for 8 hours.

TEM imaging, STEM-EDX as well as the 3D STEM-HAADF measurements were carried out using Osiris TEM equipped with FEG gun at an acceleration voltage of 200kV with Super-X Energy Dispersive X-ray Spectroscopy (EDX) detection system. Data analyses of STEM-EDX, including elemental distribution visualization, phase separation and element ratio calculation were carried out by Esprit 1.9 software. The tilt series of 3D STEM were acquired from -75° to +75° with 1.5° increments by Tomography software. The following imaging conditions were used: Spot size: 9, Magnification: 320k, Screen current: not measurable by TEM, Dose: not measurable by TEM, Acquisition time per image: 15 s. (Not measurable means that the screen current and dose were too low to be measured.)

Beam damage cannot be completely avoided but can be kept so low that it does not influence the reconstruction results. If the beam damage causes a change of morphology, the deformation can be clearly noticed after reconstruction, for example, as fuzzy cross-sections or even a feature loss. To minimize the beam damage, low screen current, low electron dose, small spot size and short acquisition

time were used. In addition, the number of acquired images per tilt series was limited by obtaining images every 1.5 degrees. The morphology of our materials, Al_2O_3, TiO_2 and MoS_2 structures was not visibly affected during the measurements and the MoS_2 slabs were clearly visible after the reconstruction. The fact that we have received a good reconstruction indicates that there was not any major damage done to the sample during the acquisition.

Tilt series were acquired for 3 larger clusters. Each cluster contained Al-rich, Ti-rich and mixed areas with variable Mo loading. The reconstructions were done in selected thin areas of these clusters with good definition of the support particles and high enough contrast for the MoS_2 slabs, all required to obtain a good quality reconstruction.

The raw tilt series data were imported to the Inspect3D software. All images were aligned using Cross Correlation tool. The volume was reconstructed using the Simultaneous Iterative Reconstruction Tomography (SIRT) method. Then the 3D stack was created. The reconstructed volume (.rec file) was then imported to the Avizo 9.0 software for the visualization purposes. The Median Filter was used for image denoising. The filtered images were used for the segmentation and labeling. Tools such as Threshold tool and TopHat tool were used for the segmentation. After different phases were labeled, the material surface was generated and different colors were used for different phases. In the end, the movie was created by the animation tool of the Avizo software.

While the acquisition of the tilt series is relatively quick, the time required for the inspection of the raw data, 3D reconstructions and visualizations is very significant indeed (4-6 days per cluster). This indicates that this technique can be applied to a limited number of interesting samples but not as a routine technique. A smart preselection of samples containing representative features, based on 2D STEM-EDX measurements, is very important.

2 Results

2.1.1 S(TEM)-EDX analysis

The used Ni-Mo/Al_2O_3-TiO_2 catalyst is heterogeneous with respect to morphology and chemical composition. An example is shown in Fig. S1. The used Ni-Mo/Al_2O_3-TiO_2 catalyst contains essentially 3 types of phases:

1. Compact mixed alumina-titania phase (P1, 46-60% of the total area), which can be described as a physical mixture of spherical titania particles (5-10 nm in diameter) and shorter alumina platelets (about 2 nm thick and between 20 and 50 nm long). This phase has a medium Ti/Al+Ti atomic ratio and is metal deficient (Table S1, Figs. S1b and S1c).
2. Highly porous alumina rich phase (P2, 30-36% of the total area), characterized by the presence of large alumina platelets (about 2 nm thick and between 50 and 150 nm long). This phase has a low Ti/Al+Ti atomic ratio and is metal rich (Table S1, Figs. S1b and S1c).
3. Compact titania rich phase (P4, 2-4% of the total area), characterized by the presence of spherical titania particles, which are 5-10 nm in diameter. This phase has a high Ti/Al+Ti atomic ratio and a medium metal content (Table S1, Figs. S1b and S1c).

Table S1. Composition of phases depicted in Figure S1c as determined by STEM-EDX

	Bulk composition	Al-Ti mix P1	Al-rich P2	Ti-rich P4
% area		46-60	30-36	2-4
Ti/Al+Ti	0.13	0.14-0.16	0.05-0.06	0.43-0.50
Mo/Al+Ti	0.11	0.07-0.09	0.15-0.20	0.09-0.13
Ni/Al+Ti	0.04	0.01-0.02	0.03-0.06	0.01-0.02
Ni/Mo	0.38	0.22-0.25	0.21-0.25	0.17-0.19
% of total Mo		33-41	52-56	2-4
% of total Ni		27-36	40-49	1-5

While a part of highly dispersed Ni on the edges of MoS_2 structures is indistinguishable in the micrographs, relatively large Ni sulfide crystals of various sizes (10-100 nm in diameter) are clearly present mixed in all three support phases (Fig. S1c: P5, corresponding to 1.7-2.8% of the total area depicted in the elemental maps and to 18-22% of the total Ni).[2] The overall S-content of the catalyst determined by (EDX) indicates that the active metals are nearly completely sulfided (91-96% as compared to MoS_2 + Ni_3S_2 stoichiometry). The S stoichiometry of the NiS_x crystals is variable, ranging from Ni_3S_2 to NiS. The other phase identified in the elemental maps is the embedding polymer (Fig. S1c: P3).

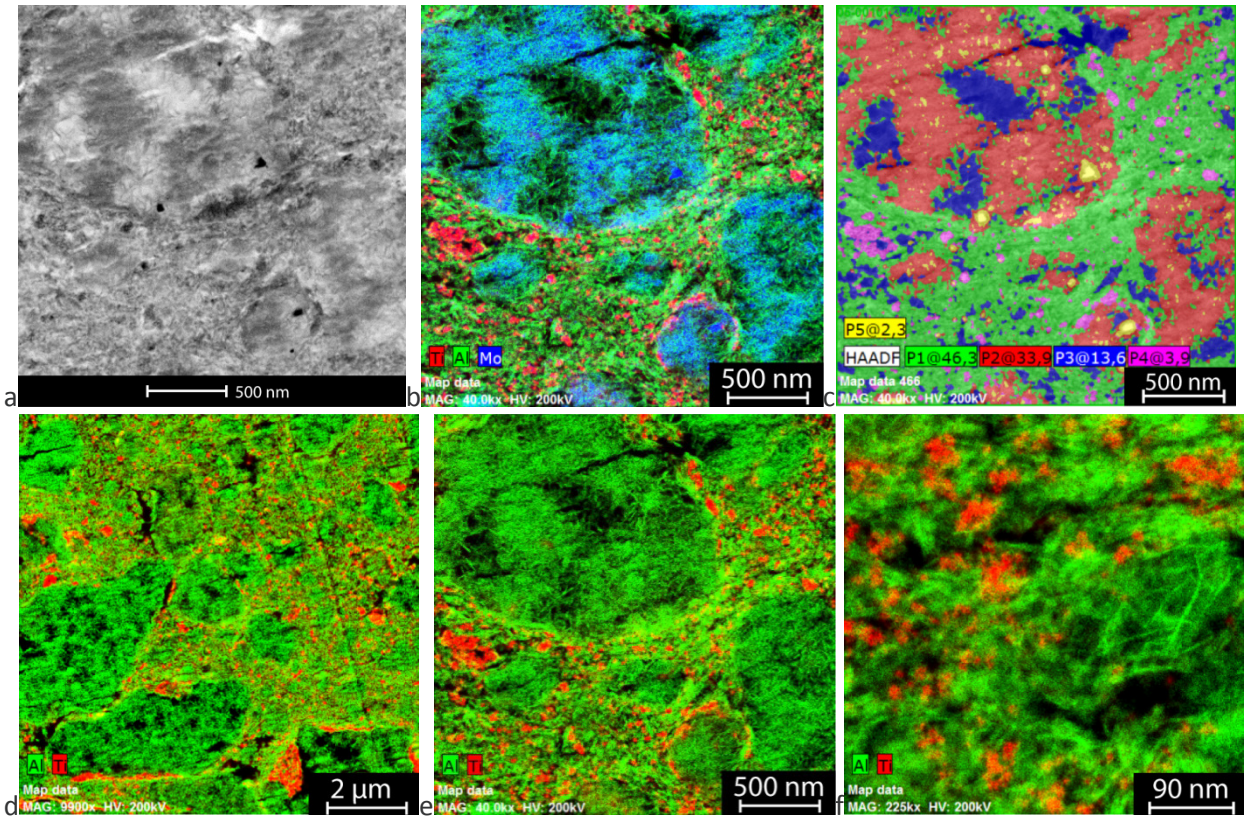

Figure S1. a. TEM micrograph, b. overlay of Mo, Al and Ti elemental maps (40k), c. corresponding phase map (40k) and overlays of Ti and Al elemental maps in 1 area at 3 magnifications d. 9.9k, e. 40k and f. 225k. (Additional information for Fig. 1 of the manuscript.)

The quantitative results of the phase analysis show that all phases (except for the Ni sulfide crystals) have similar Ni:Mo atomic ratio (Table S1, Ni/Mo is on average about 0.22). The Al-rich phase has the highest concentration of metals while the metal concentrations in the Al-Ti mixed phase and Ti-rich phase are much lower. The mixing of alumina with titania is rather heterogeneous and changes from one location to another as can be illustrated by the overlays of Ti and Al elemental maps (Figs. S1d-f).

Mo is mostly present as MoS_2 single slabs decorating the surface of the alumina platelets and the titania particles (Fig. S2). The alumina platelets are about 30 - 80 nm long and are richly decorated with MoS_2 slabs, which are between 2 and 15 nm long and appear to be lying flat on both sides of the platelets (Fig. S2b). Shorter slabs are mostly straight while longer ones may be curved if the underlying alumina is curved. The titania particles are about 10 - 15 nm in diameter and are to a large extent decorated/coated by MoS_2 slabs, which are between 2 and 15 nm long (Fig. S2c). Shorter slabs may be straight while longer ones are curved as they follow the contours of the titania particles. This implies that these structures are basal bonded on the titania surface.

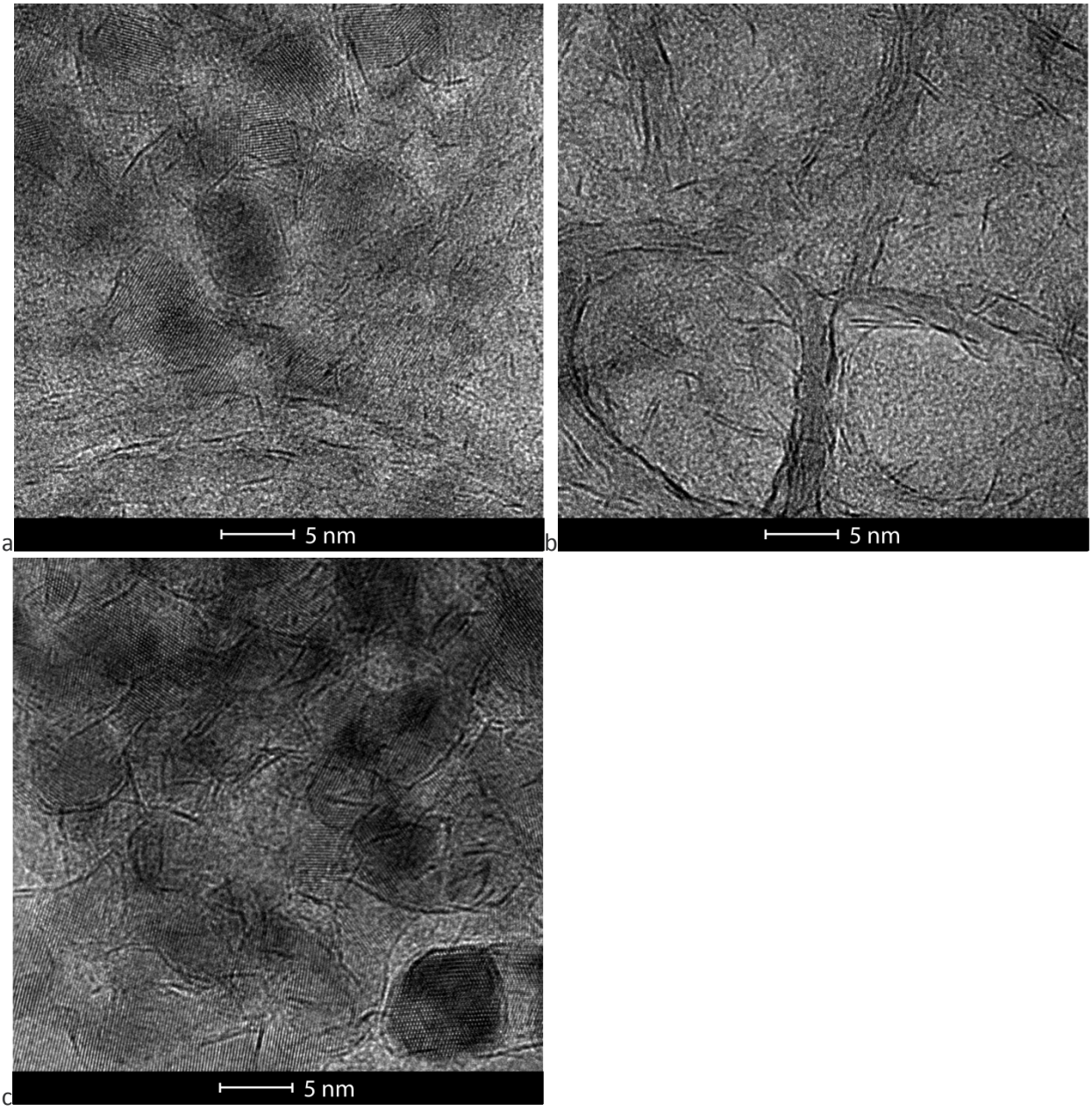

Figure S2. TEM micrographs depicting a. Al-Ti mixed phase, b. Al-rich phase and c. Ti-rich phase. (Additional information for Fig. 1 of the manuscript.)

The 2D micrographs suggest a high degree of coverage of both the alumina platelets and the titania particles with MoS_2 slabs. However, this may be for a part a product of the 2D projection of 3D information obtained from a specimen, which is about 30 nm thick.

2.1.2 3D measurements

3D STEM-HAADF provides a more detailed insight with respect to the exact size and position of the MoS_2 structures on the alumina platelets and the titania particles as well as the degree of coverage of the alumina platelets and titania particles by the MoS_2 structures. The entire cluster studied by 3D STEM-HAADF is depicted in Fig. S3.

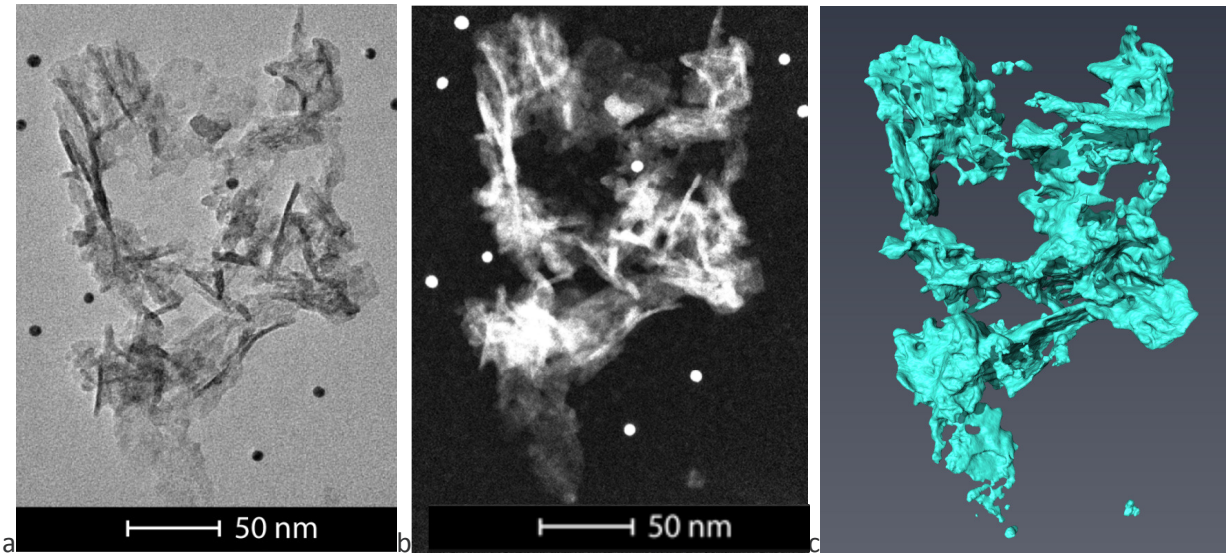

Figure S3. Cluster studied by 3D STEM-HAADF: a. TEM micrograph, b. STEM-HAADF micrograph and c. 3D visualization. The small round particles are the Au markers required for the 3D reconstruction. (Additional information for Fig. 2 of the manuscript.)

While the 2D micrographs suggest a high coverage of the alumina surface by MoS_2, the 3D results show that relatively small (3-10 nm long) isolated MoS_2 single slabs are lying flat on (= basal on) the surface of the alumina platelets in areas with low Mo content (Fig. S4). A considerable part of the alumina surface and pore volume is empty, i.e. not occupied by MoS_2 slabs. Interestingly, some MoS_2 structures seem to be sandwiched between two adjacent alumina platelets in some locations and are probably not accessible for reactant molecules. The complete 3D-visualization is included as Movie 1 in supporting evidence. MoS_2 structures are deposited inside a large cluster of alumina platelets. These clusters are still accessible for reactant molecules throughout the pores of the alumina support (Movie 1 in supporting evidence).

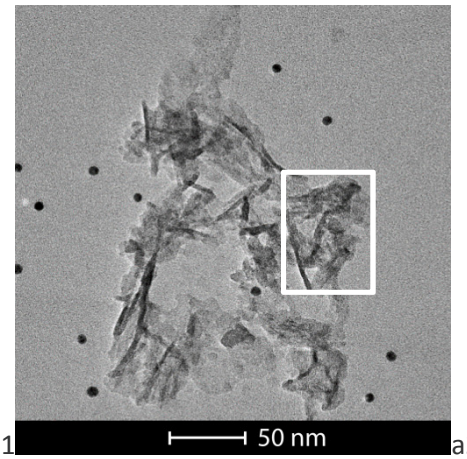

a1

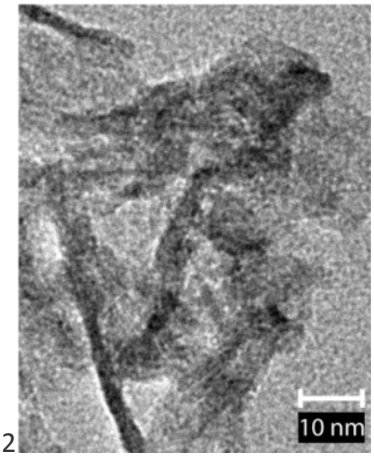

a2

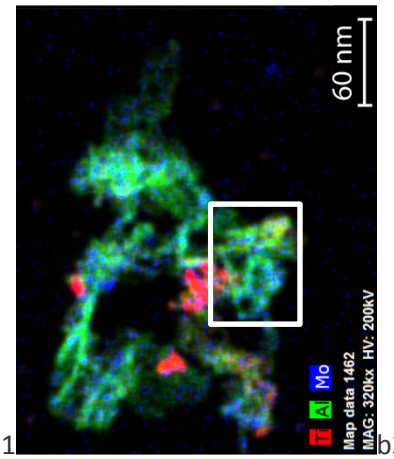

b1

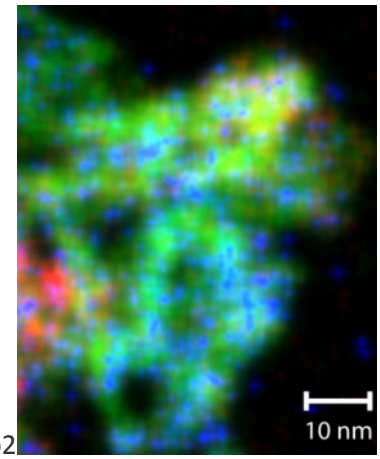

b2

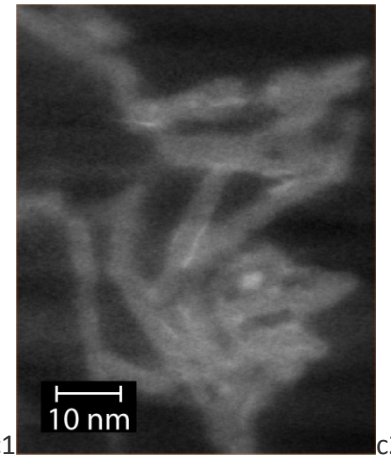

c1

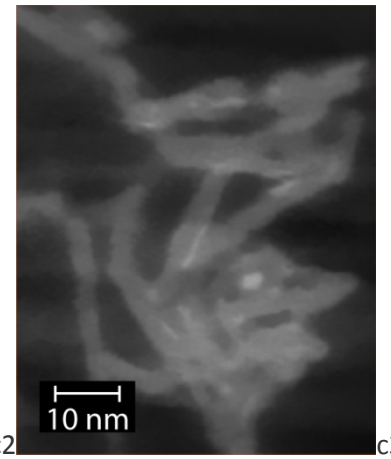

c2

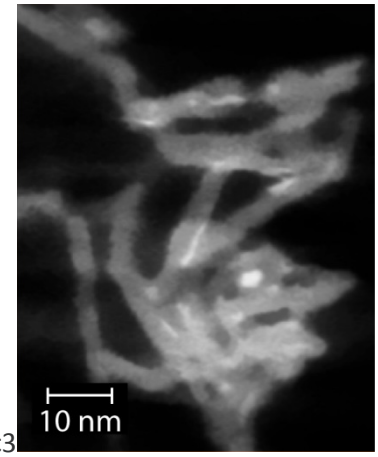

c3

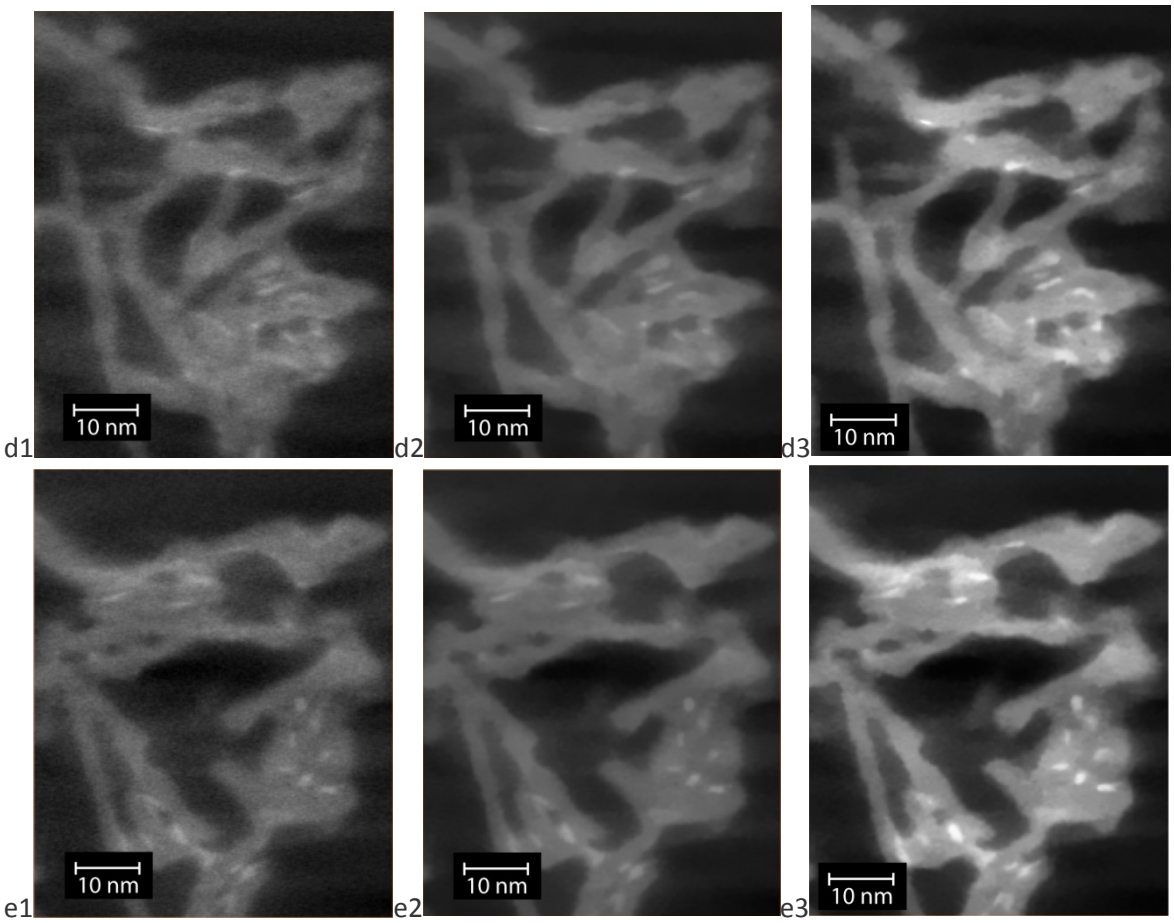

Figure S4. Cluster A: Al-rich phase with a low Mo content (Mo/Al+Ti = 0.06): a1. TEM micrograph of the entire cluster, a2. enlarged part of the micrograph showing the cluster used for reconstruction, b1. overlay of Ti-red, Al-green and Mo-blue elemental maps of the entire cluster, b2. enlarged part of the overlay showing the cluster used for reconstruction, and c-e. reconstructed slices at different Z positions [c1, d1 and e1 are the original images; c2, d2 and e2 are the corresponding filtered (= denoised) images; c3, d3 and e3 are the corresponding enhanced images (optimized contract and brightness)]. (Additional information for Fig. 2 of the manuscript.)

The MoS_2 structures are only slightly longer (5 - 10 nm long) but a much larger part of the surface of the alumina platelets is covered with MoS_2 single slabs lying flat on (= basal on) the surface of the alumina platelets in areas with higher Mo content (Fig. S5). However, a considerable part of the alumina surface and pore volume is still empty, i.e. not occupied by MoS_2 slabs. The complete 3D-visualization is included as Movie 2 in supporting evidence.

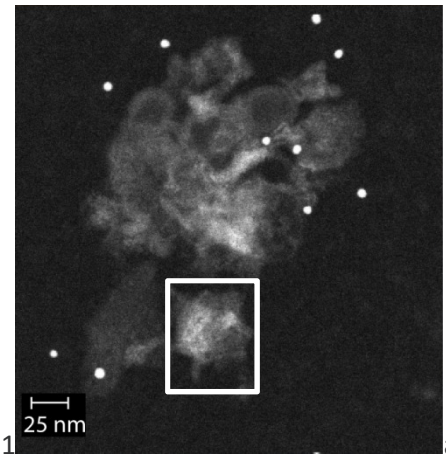

a1

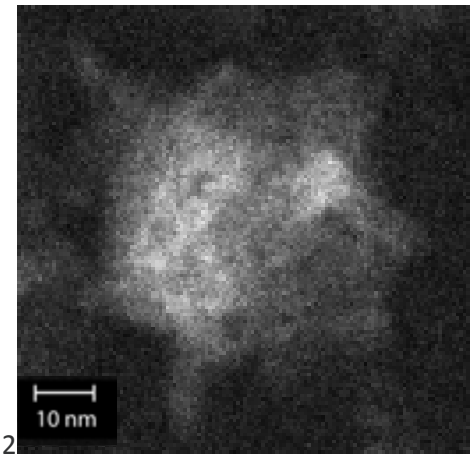

a2

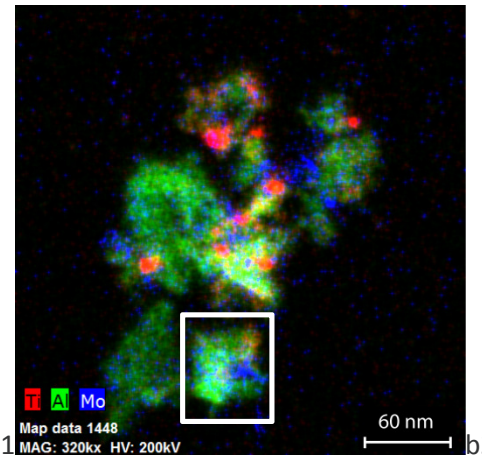

b1

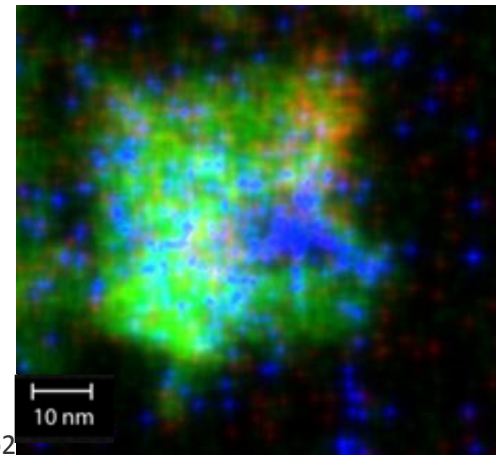

b2

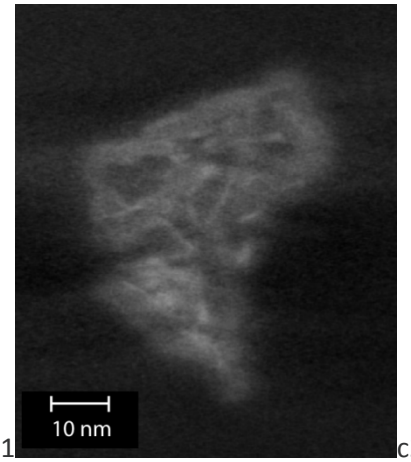

c1

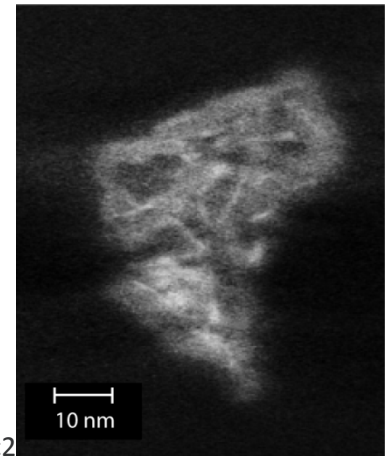

c2

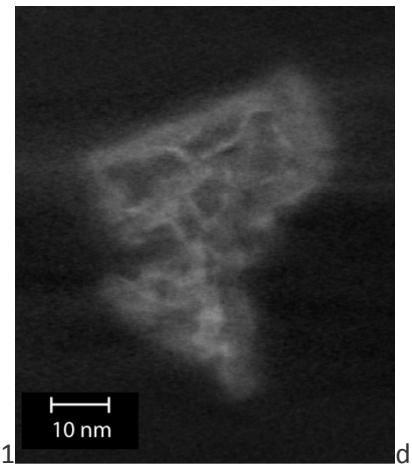

d1

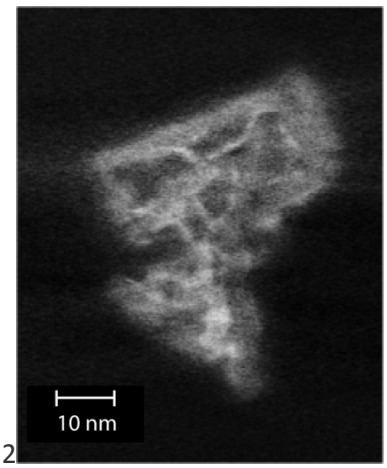

d2

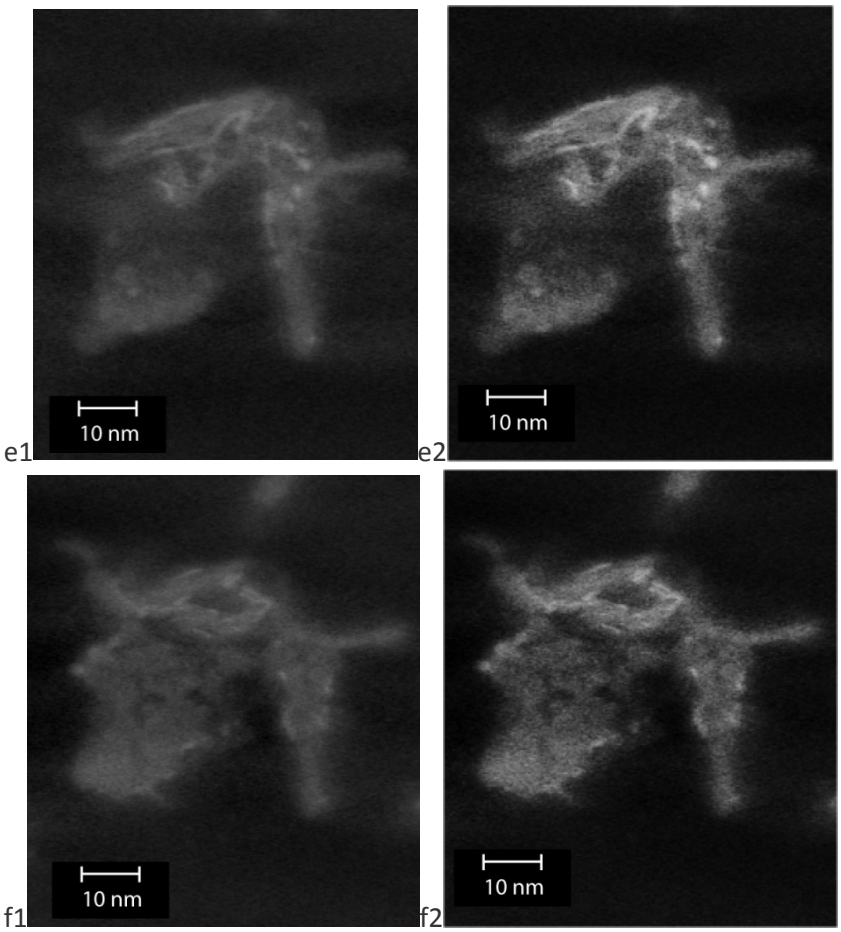

e1 e2

f1 f2

Figure S5. Cluster B: Al-rich phase with a high Mo content (Mo/Al+Ti = 0.15): a1. STEM-HAADF micrograph of the entire cluster, a2. enlarged part of the micrograph showing the cluster used for reconstruction, b1. overlay of Ti-red, Al-green and Mo-blue elemental maps of the entire cluster, b2. enlarged part of the overlay showing the cluster used for reconstruction, and c-f. reconstructed slices at different Z positions [c1, d1, e1 and f1 are the original images; c2, d2, e2 and f2 are the corresponding enhanced images (optimized contract and brightness)]. Tilt series of images corresponding to this cluster is shown in Fig. S12 in the section discussing the added value of 3D measurements. (Additional information for Fig. 3 of the manuscript.)

The 3D reconstructions of Clusters A and B shows that even though there is MoS_2 deposited in the alumina pores, the pores still seem open and accessible for reactant molecules. In addition to small pores, the material also contains large cavities in areas characterized by larger dimensions of alumina platelets. MoS_2 structures appear irregularly shaped with multiple small structures deposited on the surface of a single alumina platelet. No perfect hexagons or triangles are observed. Neighboring structures seem connected. MoS_2 structures are often bent as they follow the surface of the alumina platelets. (See also Fig. S8 in the section discussing the added value of 3D measurements.)

While the 2D micrographs suggest a high coverage of the titania particles by MoS_2 (Figs. S2c and S6a), the 3D results show that relatively small (4-12 nm long) isolated MoS_2 single slabs decorate the surface of the TiO_2 particles (Figs. S6d-S6g). The MoS_2 single slabs appear to be lying flat on (= basal on) the surface of the TiO_2 particles. Longer MoS_2 slabs follow the curvature of the TiO_2 particles. A considerable part of the titania surface is empty, i.e. not occupied by MoS_2 slabs. Interestingly, MoS_2 also seems to be sandwiched between adjacent TiO_2 particles and is perhaps less accessible for reactant molecules.

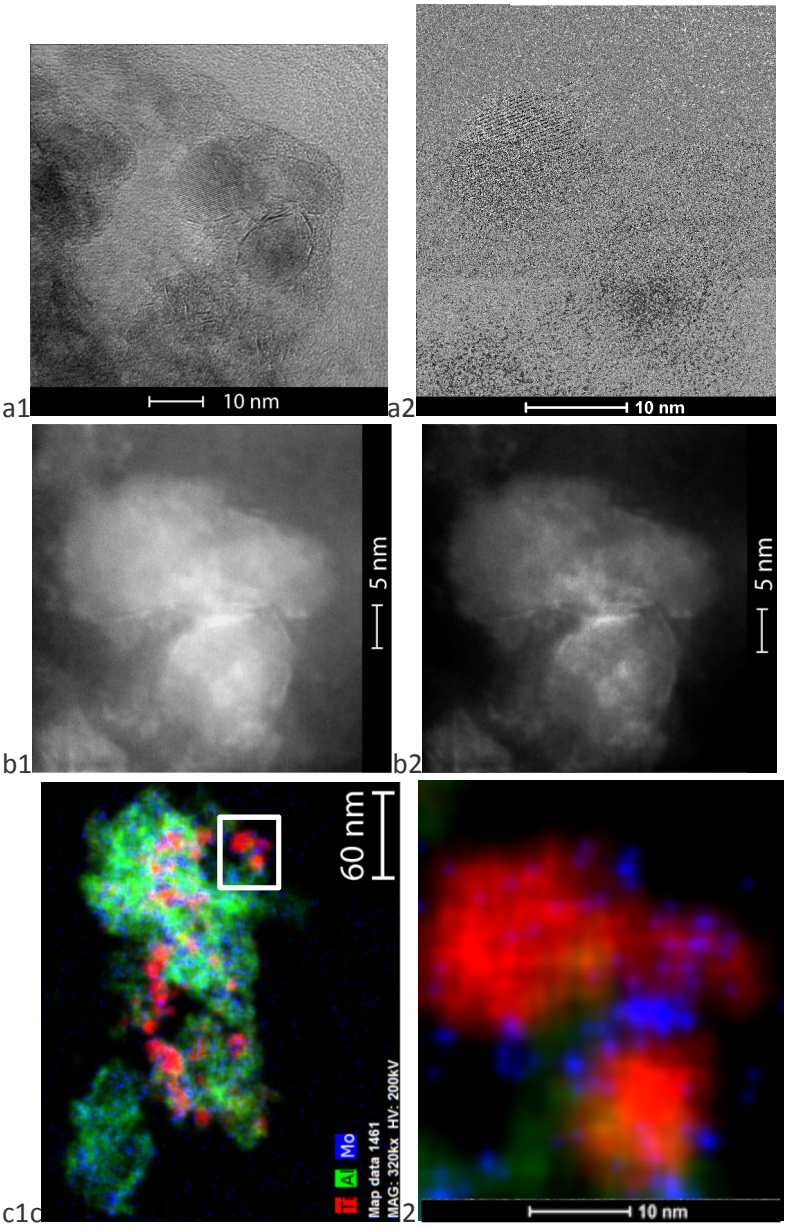

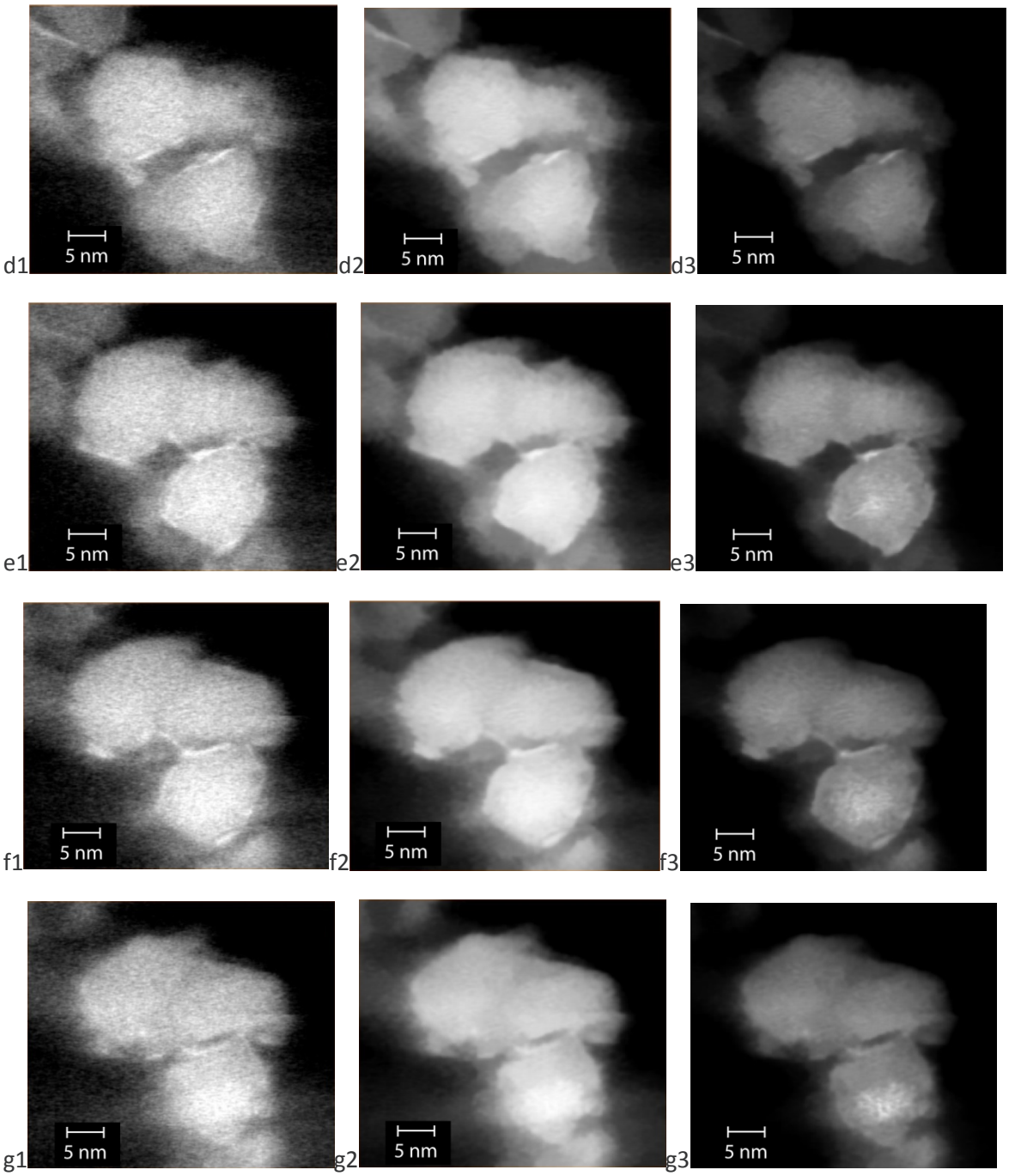

Figure S6. Cluster C: Ti-rich phase with a medium Mo content (Mo/Al+Ti = 0. 07): a1. TEM-HAADF micrograph of a larger area, a2. enlarged part of the micrograph showing the cluster used for reconstruction, b1. original STEM-HAADF micrograph of the cluster used for reconstruction, b2. corresponding enhanced image (optimized contract and brightness), c1. overlay of Ti-red, Al-green and Mo-blue elemental maps of the entire cluster, c2. enlarged part of the overlay showing the cluster used for reconstruction, and d-g. reconstructed slices at different Z positions [d1, e1, f1 and g1 are the original images; d2, e2, f2 and g2 are the corresponding filtered (= denoised) images; d3, e3, f3 and g3 are the corresponding enhanced images (optimized contract and brightness)]. (Additional information for Fig. 4 of the manuscript.)

The reconstruction of Cluster C shows that there is MoS_2 deposited on the surface of titania particles and in the cavities between the titania particles. The complete 3D-visualization is included as Movie 3 in

supporting evidence. A part of MoS_2 seems to be sandwiched between the adjacent titania particles. The voids between the particles are only partly filled and MoS_2 structures deposited therein and may still be accessible for reactant molecules. MoS_2 structures appear irregularly shaped with multiple small structures deposited on the surface of a single titania particle. A few structures resemble a perfect hexagon or a perfect triangle. Neighboring structures seem connected. MoS_2 structures are often bent as they follow the surface of the titania particles.

2.1.3 Added value of 3D measurements

When studying the support morphology, 2D micrographs often suggest that certain support particles are touching each other. For example, multiple alumina platelets and/or titania particles may appear attached to one another. 3D reconstructions show that the alumina consists of massive platelets of variable length (30 – 80 nm in diameter) and thickness (3-10 nm), which look like interconnected (Figs. S4 and S5). Titania looks like more isolated particles, having relatively narrow particle size distributions (10 - 15 nm in diameter) (Fig. S6).

In a number of TEM micrographs, MoS_2 structures may look like sandwiched between alumina platelets or between titania particles (Figs. S2b and S2c). The 3D reconstructions actually show that this is indeed the case (Figs. S4c-e an S6d-g, Movies 1 and 3 in supporting evidence). This could mean that such MoS_2 structures may be less accessible for reactant molecules.

When calculating MoS_2 dispersion from 2D-TEM micrographs, the number of MoS_2 structures, the number of layers per stack and the stack length are determined manually or by using image analysis techniques. For further calculations, it is normally assumed that the MoS_2 structures observed in TEM images are projections of perfect MoS_2 hexagons (Fig. S7a).[3] This assumption is reasonable given the hexagonal structure of MoS_2. However, triangles and ribbons as well truncated triangles and hexagons irregularly shaped structures can be present as well.[4-9]

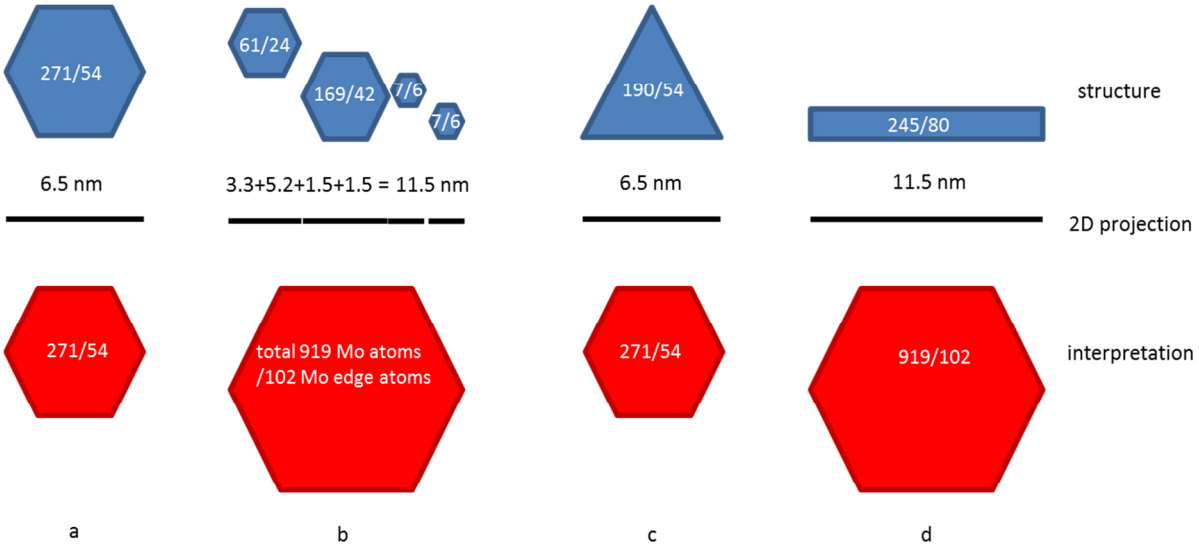

Figure S7. 2D-projection of MoS_2 structures in TEM micrographs and their interpretation in dispersion calculations: a. perfect hexagon, b. small hexagons aligned side by side on a surface of an alumina platelet, c. triangle and d. ribbon consisting of 7 rows of Mo atoms. First and second numbers in each structure give the total number of Mo atoms and the number of Mo edge atoms, respectively.

Consequently, the size of MoS_2 structures may appear much longer than they are if, e.g., several small MoS_2 structures are aligned as they decorate the surface of an alumina platelet (Fig. S7b). Moreover, a long curved MoS_2 structure may contain much less Mo atoms if it is a triangle (Figs. S7c) or a ribbon (Figs. S7d) instead of a hexagon. The numbers shown in Fig. S7 indicate that the differences between the actual structures and the interpretation based on 2D projection of a hexagon can be very large indeed (Fig. S7b: 244 versus 919 Mo atoms, Fig. S7c: 190 versus 271 Mo atoms and Fig. S7d: 245 versus 919 Mo atoms).

Furthermore, the shape of the structures is crucial when estimating the percentage of Mo atoms on the edges of the MoS_2 structures (Fig. S8). Narrow ribbons (e.g. 3-7 rows of Mo atoms) have much higher

percentage of Mo edge sites than hexagons or triangles for slab sizes above 5 nm. Mo edge sites are usually considered to be the active sites for C-S and C-N bond cleavage and are used as a measure for MoS_2 dispersion in various activity – active phase dispersion relationships.

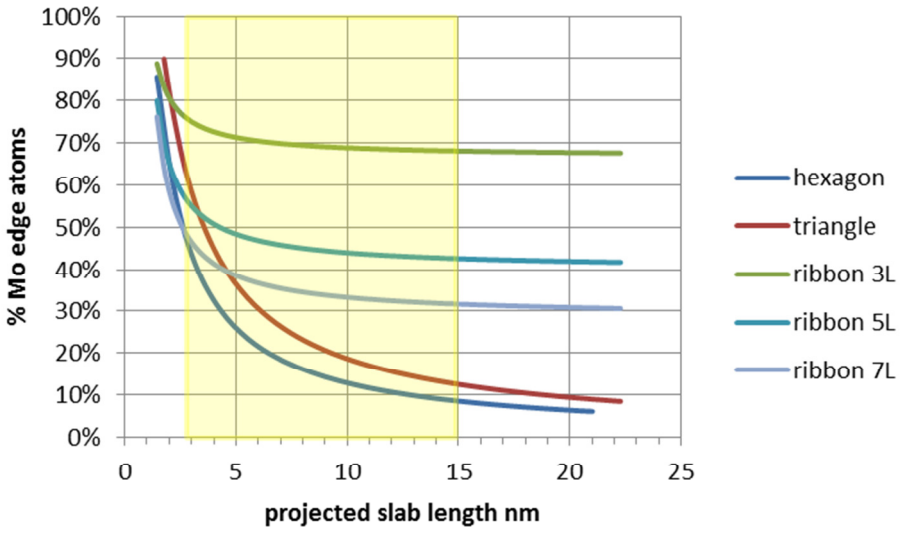

Figure S8. The percentage of Mo edge atoms as the function of structure shape (hexagon, triangle and ribbons consisting of 3, 5 and 7 rows of Mo atoms). The yellow rectangle indicates the range of MoS_2 slab sizes (2-15 nm) observed in the present sample.

An attempt was made to quantify the apparent coverage of the support by MoS_2 structures as observed in 2D measurements using a simplified model. If we assume that the MoS_2 structures are mainly aligned with the 2-dimensional Al_2O_3 platelets, we can reduce the problem to the 2D-plane. Using a random distribution of MoS_2-structures on the Al_2O_3 surface, we can then estimate the observed coverage of Al_2O_3 by MoS_2 as observed in a 2D projection when this Al_2O_3 platelet is observed side-on ($f_{observed}$). $f_{observed}$ is a function of (i) the ratio of average size of the Al_2O_3 platelets vs. the MoS_2 slabs (n) and (ii) the actual coverage of the Al_2O_3 surface by MoS_2 ($f_{coverage}$). For a simple calculation of the chance of observing a MoS_2 structure on the Al_2O_3 surface, Equation 1 is used In Fig. S9a, a representation of a 30x30 grid (representing the Al_2O_3 surface) with randomly distributed 1x1 units (MoS_2 slabs) is presented with a coverage of 33%. In Fig. S9b, the observed coverage (1 = covered, 0 = non-covered) is presented for the entire 30x30 grid and for different smaller sub-segments. It can easily be observed that the observed coverage increases with n, while at the same time the observed average size of the MoS_2 is increased.

$$f_{observed} = 1 - (1 - f_{coverage})^n \qquad \text{(Equation 1)}$$

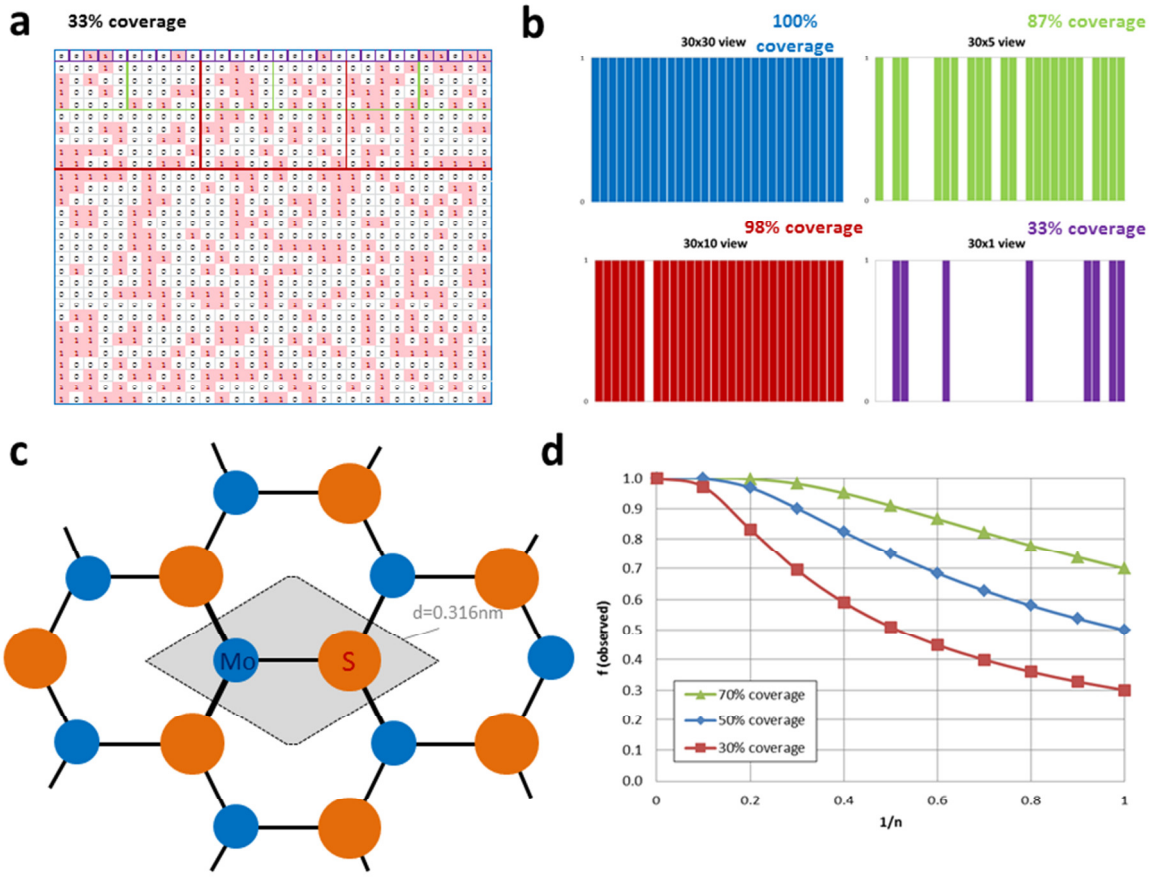

Figure S9. The estimation of surface coverage of Al_2O_3 by MoS_2 as observed in a 2D projection of a partially covered 2D-surface: a. Side-on observation of a 30x30 grid with randomly distributed 1x1 units with 33% surface coverage results in b. different observed surface coverage depending on the size of the fraction of the grid that is being observed. c. The crystal structure of MoS_2 as viewed onto the plane of a MoS_2 slab, from which the area occupied by one MoS_2 unit is calculated to be 0.086 nm^2 (grey rectangle represents the unit cell with d = 0.316 nm). d. Observed surface coverage as a function of n for different values for actual surface coverage.

An estimation for $f_{coverage}$ for the catalyst under study is obtained by using the BET surface area of the catalyst as measured by N_2-physisorption (244 m^2/g), the Mo-loading of the catalyst (20.6 wt.% MoO_3) and the area that is occupied by one unit cell in an infinite MoS_2 slab. The calculated surface-loading in the system under study is 3.6 Mo atoms/nm^2. The area occupied by one MoS_2 unit in an infinite MoS_2 crystal is 0.086 nm^2, resulting in a theoretical density of 11.6 Mo atoms/nm^2, as derived from Fig. S9c. Hence, for this system, we obtain a $f_{coverage}$ close to 0.3, which is in reasonable agreement with what is observed in the 3-D reconstructions.

For the MoO_3/Al_2O_3 system, monolayer coverage is a very common term. Upon thermal treatment, MoO_3 is known to spread over the Al_2O_3 surface resulting in a MoO_3 overlayer. Only when monolayer coverage is reached, crystalline MoO_3 phases are observed, e.g. using X-ray diffraction. The reported observed maximum monolayer coverage is in the range of 5 Mo atoms/nm^2,[2,10] which is significantly lower than the theoretical maximum coverage of Al_2O_3 by MoS_2 as calculated above. This is probably due to the Al-O-Mo bonds that are formed upon calcination in the MoO_3/Al_2O_3 system. Maximum monolayer coverage for the oxidic catalyst is limited by the number of anchor sites for Mo on the Al_2O_3 surface rather than the space available on this surface for the MoO_3 phase.

As an estimation of n, we use a factor 5, based on the size of the Al_2O_3 platelets (20-60 nm) and MoS_2 slabs (5-10 nm). From the plot of the observed % coverage versus 1/n, as shown in Fig. S9d, we derive that in 2D projections of the Al_2O_3 platelets, at 30% actual coverage, >80% of the Al_2O_3 surface will appear to be covered by MoS_2, which is a significant over-estimation of the actual value.

The 3D reconstructions show that MoS_2 structures are irregularly shaped with multiple small structures deposited on the surface of a single alumina platelet (Figs. S10 and S14) or a single titania particle (Figs. S11-S13). A few structures resemble a perfect hexagon or a perfect triangle (Fig. S11). Neighboring structures seem connected (Figs. S10 and S12). MoS_2 structures are often bent (Figs. S10-S14) as they follow the surface of underlying alumina platelets or titania particles. Curved MoS_2 structures may appear smaller in 2D projections if only parts of such structures are oriented parallel to the electron beam (Fig. S14) etc.

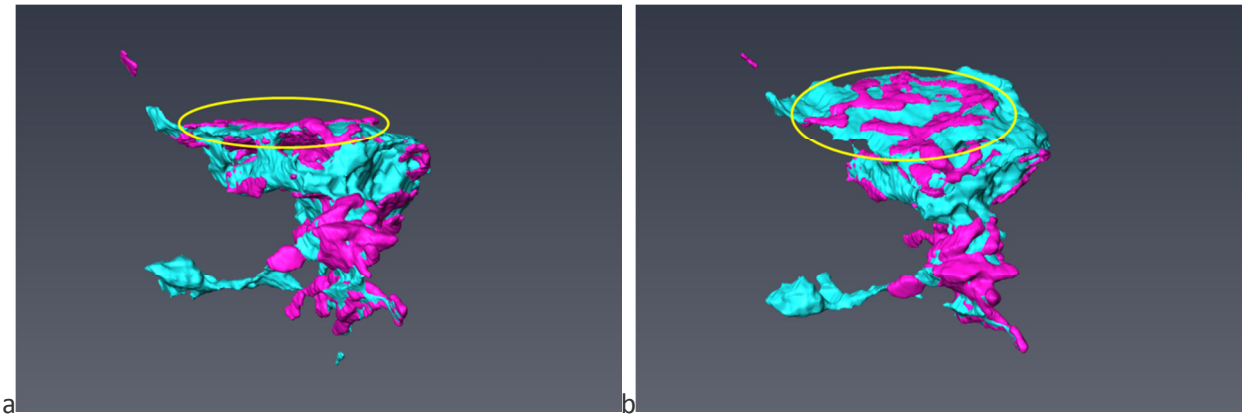

Figure S10. Cluster B: Al-rich phase with a high Mo content (Mo/Al+Ti = 0.15): Several small MoS_2 structures are aligned as they decorate the surface of an alumina platelet: a. aligned structures look like a long MoS_2 slab and b. separate small ribbon-like structures are deposited on the surface of a large alumina platelet. Neighboring structures seem connected. MoS_2 structures are often bent as they follow the surface of the alumina platelets. (Additional information for Fig. 3 of the manuscript.)

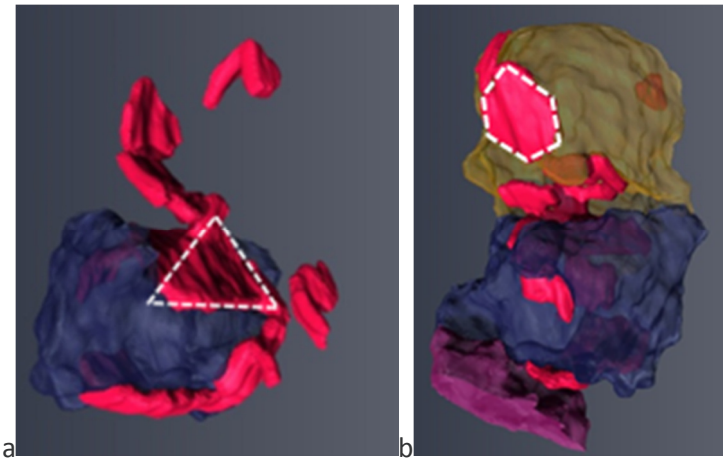

Figure S11. 3D-visualization of cluster C seen from different angles. A few structures resemble a perfect hexagon or a perfect triangle. Indications of the MoS_2 shape are merely intended to guide the eye. (Additional information for Fig. 4 of the manuscript.)

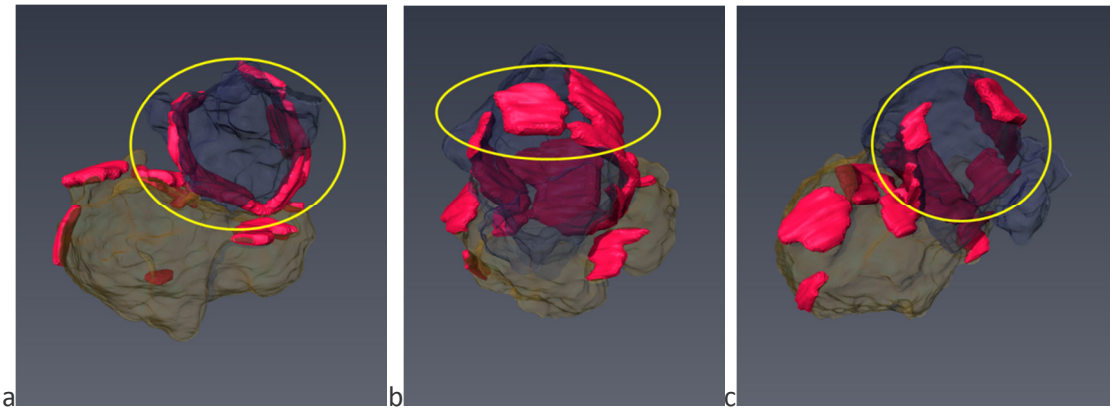

Figure S12. Cluster C: Ti-rich phase with a medium Mo content (Mo/Al+Ti = 0. 07): The apparent degree of coverage of the dark blue titania particle changes depending on the orientation towards the electron beam. Curved MoS_2 structures may appear smaller in 2D projections if only parts of such structures are oriented parallel to the electron beam. a. Except for a small gap, the titania particle seems fully coated by curved MoS_2 layers, b. the gap is invisible at this orientation and c. only a part of the curved layers is visible at this orientation. (Additional information for Fig. 4 of the manuscript.)

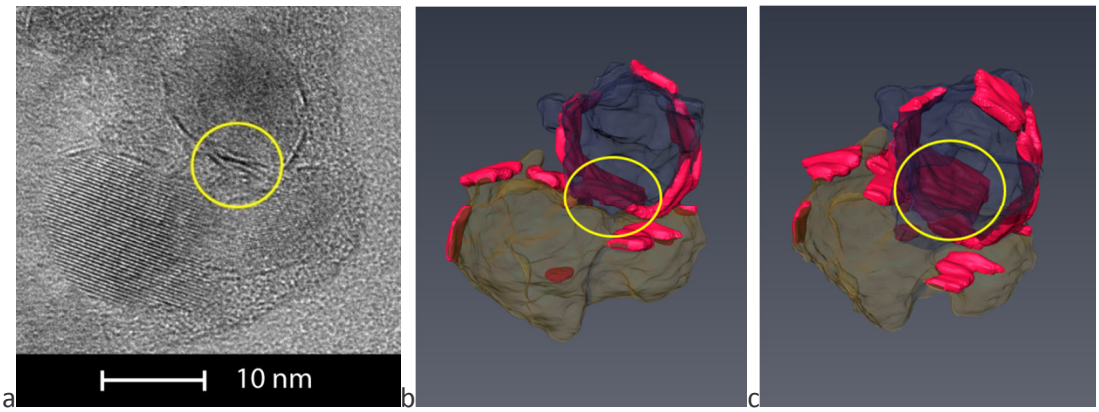

Figure S13. Cluster C: Ti-rich phase with a medium Mo content (Mo/Al+Ti = 0. 07): a. TEM micrograph, b. and c. 3-D visualization viewed from different directions. Separate MoS_2 slabs may appear as a stack in the 2D projection. (Additional information for Fig. 4 of the manuscript.)

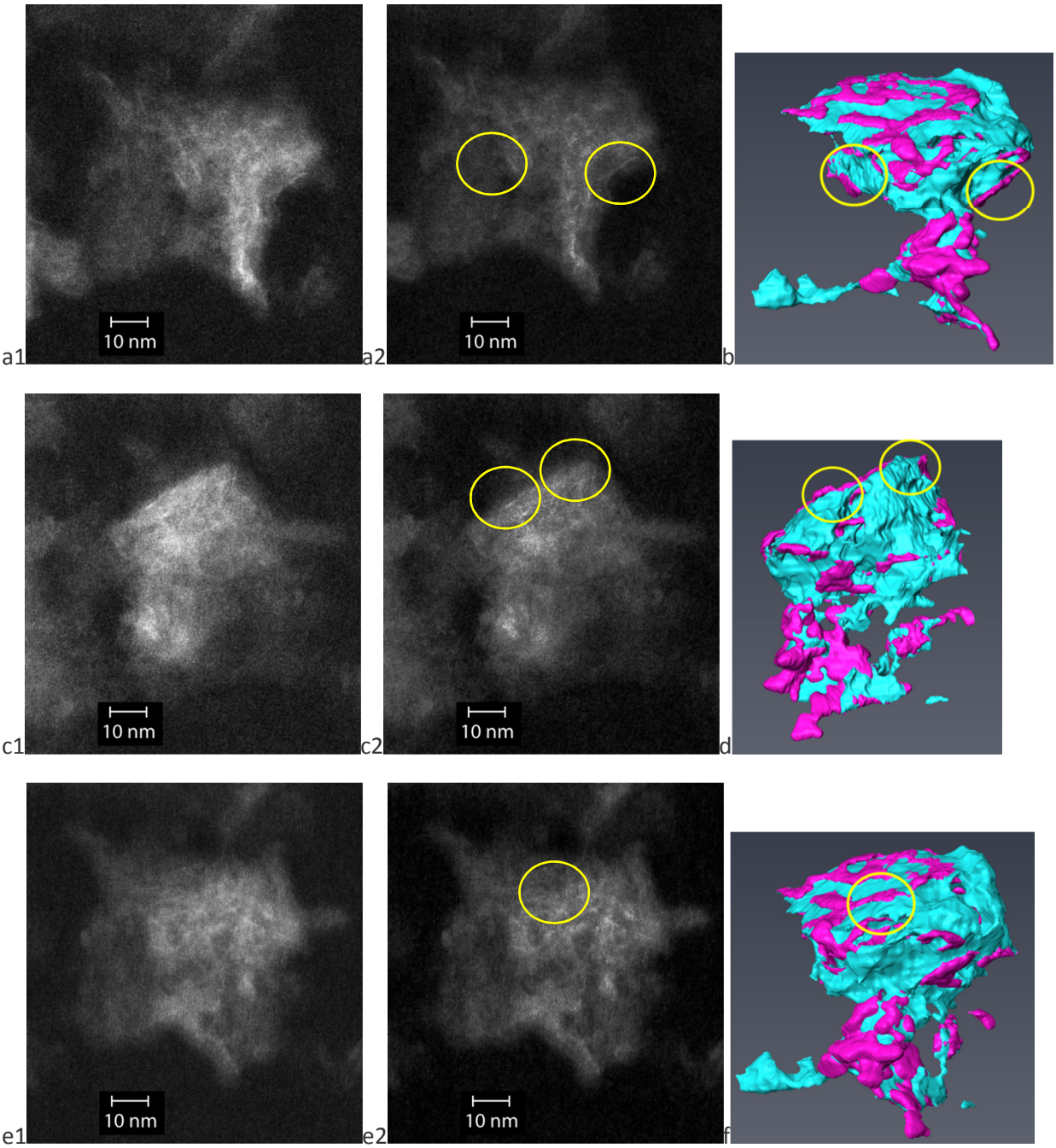

Figure S14. Cluster B: Al-rich phase with a high Mo content (Mo/Al+Ti = 0.15): Tilt series of images showing that MoS_2 structures appear and disappear as the cluster is tilted: a and b. - 30 degree, c. and d. 45 degree and e. and f. 0 degree [a1, c1, and e1 are the original images; a2, c2 and e2 are the corresponding enhanced images (optimized contract and brightness)]. (Additional information for Fig. 3 of the manuscript.)

3 References

(1) Topsoe, N. Y.; Topsoe, H. *J. Catal.* **1993**, 139, 631–640.
(2) Eijsbouts, S.; van den Oetelaar, L. C. A.; van Puijenbroek, R. R. *J. Catal.* **2005**, 229, 352–364.
(3) Eijsbouts, S.; Heinerman, J. J. L.; Elzerman, H. J. W. *Appl. Catal. Gen.* **1993**, 105, 53–68.
(4) Deepak, F. L.; Esparza, R.; Borges, B.; López-Lozano, X.; Jose-Yacaman, M. *Catal. Lett.* **2011**, 141, 518–524.
(5) Hansen, L. P.; Ramasse, Q. M.; Kisielowski, C.; Brorson, M.; Johnson, E.; Topsøe, H.; Helveg, S. *Angew. Chem. Int. Ed.* **2011**, 50, 10153–10156.
(6) Carlsson, A.; Brorson, M.; Topsøe, H. *J. Catal.* **2004**, 227, 530–536.
(7) Baubet, B.; Devers, E.; Hugon, A.; Leclerc, E.; Afanasiev, P. *Appl. Catal. Gen.* **2014**, 487, 72–81.
(8) Baubet, B.; Girleanu, M.; Gay, A.-S.; Taleb, A.-L.; Moreaud, M.; Wahl, F.; Delattre, V.; Devers, E.; Hugon, A.; Ersen, O.; Afanasiev, P.; Raybaud, P. *ACS Catal.* **2016**, 6, 1081–1092.
(9) Girleanu, M.; Lopes Silva, S.; Ihiawakrim, D.; Chaumonnot, A.; Bonduelle-Skrzypczak, A.; Lefebvre, F.; Dufaud, V.; Gay, A.-S.; Ersen, O. *Micropor. Mesopor. Mat.* **2015**, 217, 190–195.
(10) Leyrer, J.; Zaki, M. I.; Knoezinger, H. *J. Phys. Chem.* **1986**, 90, 4775–4780.